ASFM: Augmented Social Force Model for Legged Robot Social Navigation

Sebastian Ægidius[1], Rodrigo Chacón-Quesada[2], Andromachi Maria Delfaki[1], Dimitrios Kanoulas[1], and Yiannis Demiris[2]

***Abstract*— Social navigation in robotics primarily involves guiding mobile robots through human-populated areas, with pedestrian comfort balanced with efficient path-finding. Although progress has been seen in this field, a solution for the seamless integration of robots into pedestrian settings remains elusive. In this paper, a social force model for legged robots is developed, utilizing visual perception for human localization. In particular, an augmented social force model is introduced, incorporating refined interpretations of repulsive forces and avoidance behaviors based on pedestrian actions, alongside a target following mechanism. Experimental evaluation on a quadruped robot, through various scenarios, including interactions with oncoming pedestrians, crowds, and obstructed paths, demonstrates that the proposed augmented model significantly improves upon previous baseline methods in terms of chosen path length, average velocity, and time-to-goal for effective and efficient social navigation. The code is open-source, while video demonstrations can be found on the project's webpage: `https://rpl-cs-ucl.github.io/ASFM/`**

I. INTRODUCTION

Navigating through human-populated environments, such as urban streets or shopping centers, presents a complex challenge in robotics, requiring the combination of intricate prediction of human behavior with effective route planning. Unlike traditional robotics navigation [1], which primarily addresses static or dynamically predictable obstacles, social navigation requires the integration of interaction between humans and robots to maneuver through spaces actively shaped by human presence. This approach significantly relies on visual input, a dominant human sensory channel, which is increasingly being used in robotics through advanced neural networks and enhanced computational capacities [2].

Current social navigation models, mainly developed for interaction, such as tour guides or information assistants [3], lack the agility and adaptability needed for seamless integration into everyday human environments. In contrast, modern agile robots, particularly quadrupeds [4], [5], offer notable benefits in these settings, navigating more naturally among pedestrians. However, their deployment faces significant hurdles due to safety and social acceptance concerns, despite the great potential offered by advancements in robotic perceptual and interaction capabilities.

Fig. 1: Social navigation examples, based on the Augmented Social Force Model (ASFM), handling oncoming pedestrians (left) and following people through crowded areas (right).

Despite these technological strides, a significant gap persists in the seamless integration of robots into these social contexts, primarily due to human discomfort and apprehension in sharing walking spaces with robots as equals. This unease underscores a critical challenge in the development of social navigation systems for robots: the need for models that not only ensure safety and efficiency, but also exude friendliness and minimize intrusion into personal space. Addressing this challenge, our article introduces a novel social navigation model designed to harmonize robot movement within human-centric environments (Fig. 1), with the aim of bridging the comfort gap and foster more naturalistic interactions between humans and robots.

We demonstrate our social navigation algorithm on a physical quadruped robot system operating in human populated mock environments. Our approach is capable of social navigation with a focus on non-intrusive human-robot interaction, with main contributions being the introduction of an Augmented Social Force Model (ASFM) that improves upon the notion of potential force fields describing pedestrian intentions, implemented on a mobile robot system that couples perception and action for autonomous non-intrusive vision-based pedestrian social navigation.

[1]Sebastian Ægidius, Andromachi Maria Delfaki, and Dimitrios Kanoulas are with the Robot Perception and Learning Lab, Department of Computer Science, University College London, Gower Street, WC1E 6BT, London, UK. Dimitrios Kanoulas is also with the AI Centre, Department of Computer Science, UCL and the Archimedes/Athena RC, Greece. {s.aegidius, andromachi.delfaki.23, d.kanoulas}@ucl.ac.uk

[2]Rodrigo Chacón-Quesada and Yiannis Demiris are with the Personal Robotics Lab, Department of Electrical and Electronic Engineering, Imperial College London, SW7 2AZ, London, UK. {r.chacon-quesada17, y.demiris}@imperial.ac.uk

This work was supported by the UKRI FLF [MR/V025333/1] (RoboHike), UKRI grant [EP/V026682/1], and RAEng Chair in Emerging Technologies to YD.

A. Related Work

Social navigation, a field that combines human behavioral analysis with robotic navigation, has seen significant advances, particularly influenced by autonomous driving technologies. The challenges in social navigation include motion planning, human behavior interpretation, and model evaluation, with safety and social compliance being paramount. An overview of previous methods and approaches to social navigation can be found in [6].

Historically, path planning treated humans as static entities, lacking interaction [7]–[16]. Contemporary approaches, however, prioritize human awareness, inferring intention, and responses to enhance social navigation [17], [18]. This shift led to the adoption of models based on Inverse Reinforcement Learning (IRL), focusing on human interaction and predictive planning [19]. Notably, Cooperative Collision Avoidance models emphasize collective effort in multi-agent environments to mitigate collisions, underscoring the complexity of human behavior interpretation [20]. Different methodologies have emerged that combine explicit and implicit strategies for social compliance. Explicit approaches, such as those that use topological invariants and braid groups, simplify multi-agent dynamics for improved path planning [21], [22]. Meanwhile, implicit models, typically grounded in neural networks, adapt based on learned collision avoidance behaviors without explicit constraints, aligned with IRL paradigms to navigate ambiguous human behaviors [23], [24]. A most notable work using Reinforcement Learning (RL) for modeling and navigating pedestrian populated environments is the work by Chen et al. [25], where they postulated that its relatively easier to train on what social norms dictate not to do, an approach this work was influenced by when creating solutions for certain common pedestrian scenarios. More recently, Hirose et al. [26], also introduced a learning-based way to train a policy for unobtrusive social navigation for simple social interactions. Recent innovations include Mixed Observability Markov Decision Processes and Partially Observable Markov Decision Processes, along with applications of Generative Adversarial Networks and Long Short-Term Memory networks [27]–[29]. These models, particularly prevalent in the autonomous driving sector, have contributed significantly to understanding social navigation within densely populated environments.

Although learning-based methods described above are able to learn complex behaviors of high dimensionality and rich data, interpretability, simplicity, efficiency, and robustness are sometimes lacking. The evolving landscape of social navigation underscores the necessity for multifaceted solutions that integrate behavioral insights and advanced computational techniques, highlighting the absence of a one-size-fits-all model architecture for effective social navigation. These challenges are addressed in this paper by developing and implementing an advanced Social Force Model [30] on a quadruped robot, leveraging visual perception for enhanced human detection and interaction. By synthesizing elements of traditional and social navigation, a solution is presented that not only avoids obstacles, but also engages with pedestrians in a manner that respects social norms and enhances pedestrian comfort. Social comfort is regarded on the grounds that the pedestrians in the scenarios did not have to make way for the robot and were not socially intruded upon by the robot. Onboard visual sensors are used for social navigation, compared to previous works that use external bird-eye-view cameras, e.g. [31], making much of the state-of-the-art pedestrian intention descriptions and algorithms inapplicable to a first-person Point of View (POV) robot. Other works, such as [32], apply a first-person POV for predicting pedestrian movement, although they fall outside the immediate scope of this paper, which is aimed at exploring the interaction between pedestrians and robots rather than predicting the interaction scenario. Closer to this work is [33], which proposed a headed SFM to deal with side-stepping, following behavior, and direction priorities, as well as [34], [35], which use elliptical forces for robot social navigation to overcome the use of limit cycles. A step forward is taken with the integration of an augmented SFM with refined repulsive forces and avoidance behaviors, significantly enhancing path efficiency and pedestrian comfort in various challenging scenarios on legged robots.

II. PEDESTRIAN DYNAMICS MODELING

In this section, the background theory is given, which allows a legged robot socially navigate among humans, extending upon the notion of Social Force Model (SFM) for pedestrian dynamics by Helbing et al. [30] as the main dynamics of human-to-human interaction. SFM describes a pedestrian's intentions to reach a goal location, while avoiding other pedestrians, through attractive (goal) and repulsive (pedestrian and obstacles) forces. The final or immediate next goal location is formulated as the attractive force acting on the pedestrian. The attractive force influencing pedestrian α is described by the following equation:

$$\mathbf{F}_{\alpha}^{attr}(v_{desired}, \hat{\mathbf{e}}, \mathbf{v}_{\alpha}) = \frac{1}{\tau}(v_{desired}\hat{\mathbf{e}} - \mathbf{v}_{\alpha}). \tag{1}$$

where τ is a force relaxation factor (called relaxation time), $v_{desired}$ is the desired maximum speed the pedestrian wants to reach, $\hat{\mathbf{e}}$ is the unit vector of the desired direction towards the field source (i.e., the pedestrian or the goal point), and $\mathbf{v}_{\alpha}$ is the current velocity of the pedestrian. Eq. 1 can be thought of as an acceleration. When $\mathbf{v}_{\alpha} = \mathbf{0}$, then $\mathbf{F}_{\alpha}^{attr}$ is maximized, while when $\mathbf{v}_{\alpha} = v_{desired}\hat{\mathbf{e}}$, then $\mathbf{F}_{\alpha}^{attr} = \mathbf{0}$ with no further velocity increase. The relaxation time given by τ is what is responsible for a slower increase in velocity based on the force or as it decreases the overall acceleration.

The repulsive forces deployed by the model come from other pedestrians and barriers, where they all exert a force directed away from themselves. This force from pedestrian β onto pedestrian α is represented by the following equation:

$$\mathbf{F}_{\alpha\beta}(d_{\alpha\beta}) = -\nabla_{\mathbf{d}_{\alpha\beta}} V_{\alpha\beta}[b(d_{\alpha\beta})]. \tag{2}$$

where $d_{\alpha\beta}$ is the distance between pedestrian α and β, $\nabla_{d_{\alpha\beta}}$ is the gradient of the field emitted by a pedestrian at the

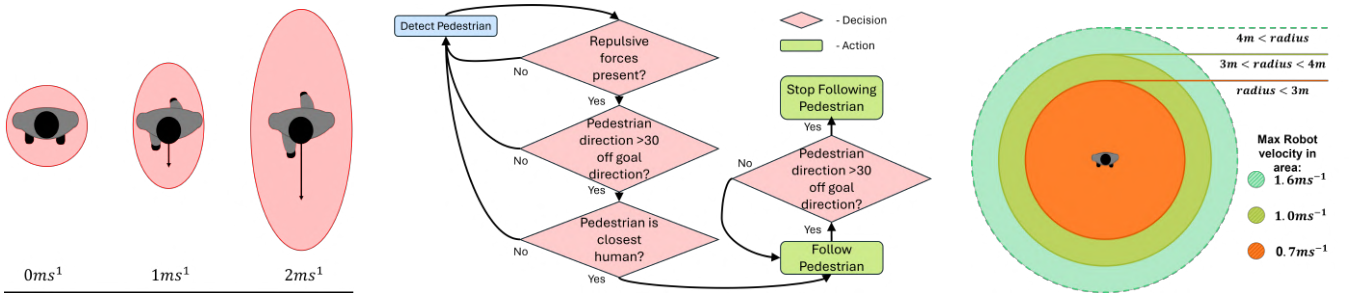

(a) (b) (c)

Fig. 2: (a) The change in repellent force field of a pedestrian proportional to its movement speed: a circle when at rest and an elongating ellipsoid with higher velocity. (b) The conditions for the follow behavior. The value of 30 degrees was chosen based on experimental trials. (c) The maximum forward velocity allowed depending on how far away the closest pedestrian is. The values seen are all chosen based on experimental trial data and pedestrian comfort feedback.

given distance, V is an exponential decreasing function with respect to b taking the shape of an ellipse, given by

$$V_{\alpha\beta}(b) = Ae^{-b/B}. \tag{3}$$

where A and B are parameters to tune based on how much the exponential decrease of the field should be, originally set to $V_{\alpha\beta}(b) = 2.1e^{-b/0.3}$, b represents the semi-minor axis of the ellipse the pedestrian is surrounded by when moving with some velocity, and is given by

$$2b = \sqrt{(||d_{\alpha\beta}|| + ||d_{\alpha\beta} - v_\beta \Delta t \mathbf{e}_\beta||)^2 - (v_\beta \Delta t)^2}. \tag{4}$$

where the term $v_\beta \Delta t$ signifies the step size of pedestrian β. The ellipse grows in size the higher pedestrian β's speed is, but does not change shape with a fixed semi-minor to semi-major ellipse axis ratio. Then, incorporating Eqs. 3 and 4 into Eq. 2, the repulsive force for pedestrians α and β can be rewritten into a more descriptive format

$$\mathbf{F}_{\alpha\beta}(d_{\alpha\beta}) = \tag{5}$$
$$Ae^{\frac{-b_i}{B}} \frac{||d_{\alpha\beta_i}|| + ||d_{\alpha\beta_i} - \mathbf{Y}_i||}{4b_i} \left(\frac{d_{\alpha\beta_i}}{||d_{\alpha\beta_i}||} + \frac{d_{\alpha\beta_i} - \mathbf{Y}_i}{||d_{\alpha\beta_i} - \mathbf{Y}_i||}\right).$$

Moreover, one could think of walls and borders to have a similar repulsive effect on pedestrians, with an additional repulsive force between pedestrian α and border B

$$\mathbf{F}_{\alpha B}(d_{\alpha B}) = -\nabla_{\mathbf{d}_{\alpha B}} U_{\alpha B}(||d_{\alpha B}||). \tag{6}$$

where $U_{\alpha B}$ is another decreasing exponential function as in Eq. 3 tuned for walls and borders.

The direction of pedestrian motion also influences the forces. As the social force formulas hold proper effectiveness if observed in the desired direction, unwanted influence from other directions can be handled by a direction dependent weighting function

$$w(\hat{\mathbf{e}}, \mathbf{F}) = \begin{cases} 1 & \text{if } \hat{\mathbf{e}} \cdot \mathbf{F} \geq \mathbf{F}cos(\phi) \\ c, & \text{otherwise,} \end{cases} \tag{7}$$

where $\hat{\mathbf{e}}$ is the unit vector, $0 < c < 1$ weakens forces acting behind the pedestrian, and ϕ is set based off of the effective angle of vision (2ϕ).The final SFM can be formulated as the summation of all the aforementioned forces:

$$\mathbf{F}_\alpha = \mathbf{F}_\alpha^{attr}(v_{desired}, \hat{\mathbf{e}}, \mathbf{v}_\alpha) + \sum_\beta w(\mathbf{e}, \mathbf{F}_{\alpha\beta}) \mathbf{F}_{\alpha\beta}(d_{\alpha\beta}) \tag{8}$$
$$+ \sum_B w(\mathbf{e}, \mathbf{F}_{\alpha B}) \mathbf{F}_{\alpha B}(d_{\alpha B}).$$

The SFM depends on a strong assumption that all pedestrians follow the exact same principles when interacting, making it difficult to be applied in the real-world. In particular, it is hard to expand elliptical pedestrian personal space shape, it has non-intuitive backwards motion when pushed head on, it does not have particular awareness of human formations, and it is a poor practical solution for lowering repulsive forces using the direction dependent weighting function. This paper, aims at overcoming this assumption with a novel Augmented Social Force Model (ASFM), a robot-pedestrian model more obedient to human movement as opposed to two way human-robot interaction grounded in the assumption that currently most humans are not accustomed to interacting with a robot pedestrian.

III. METHODOLOGY

In this section, the Augmented Social Force Model (ASFM) is presented, augmenting the previously described SFM model. In this way, the assumption that all humans navigate with the same social primitives is avoided. Five augmentations are proposed, detailed in the following subsections, to allow for more obedient behavior of a robot navigating around humans, overcoming the major drawbacks of the SFM.

*1) **Pedestrian Personal Space**:* First, the model is augmented with force fields that are more robust and utilize the limited first-person POV of a pedestrian. Holding onto the elliptical force field shape of pedestrians as in the original SFM, the model is made more responsive by reformulating the repulsive force from pedestrians into a static force and a moving force. Thus, the repulsive force is redefined as

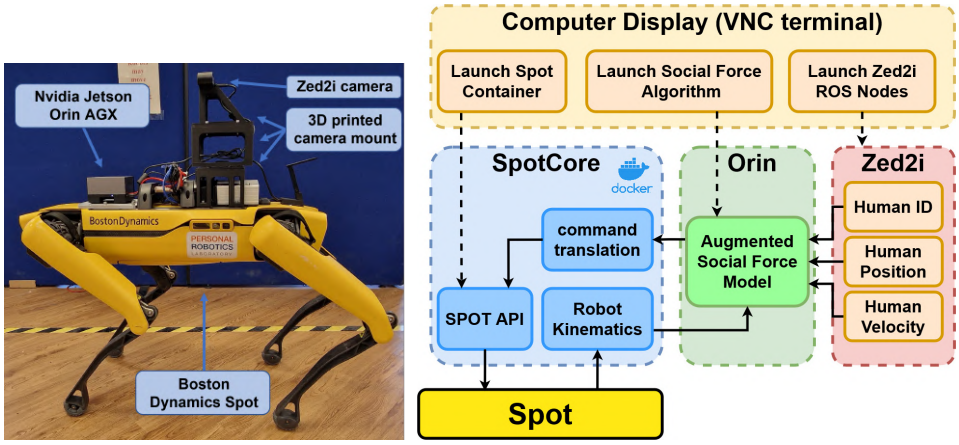

Fig. 3: The legged robotic system deployed: a Boston Dynamics Spot quadruped robot, an NVIDIA Jetson Orin AGX, and a mounted Zed2i RGB-D camera, accompanied by a system integration diagram as implemented on the robot.

follows:

$$F_{\alpha\beta-static} = Ae^{Bx+C} \tag{9}$$

$$F_{\alpha\beta-moving} = Ae^{(x-d)B+C}, \tag{10}$$

where A, B, and C are hyper parameters to create a force field that will allow for smoother encounters than in Eq. 3 and d is the distance from the ellipse centroid to the point on the ellipse closest to the robot. As the magnitude of a radial force field is the same for a set distance away from the center, the x in Eq. 10 represents the distance from the pedestrian to the robot. The distance d is in turn created from the measured velocity of the pedestrian observed. The higher the velocity, the more the ellipse axes grow. The rate of growth is independent between the semi-minor and the semi-major axis. Helbing's notion of step size, specific for each pedestrian, is difficult to translate to real world and further motivated the change in the pedestrian repulsive forces. A visualization of what the pedestrian personal space fields can be seen in Fig. 2a.

*2) **Side-Stepping**:* The second augmentation developed for the ASFM is a conversion of resistance to sideways motion as opposed to decreased motion or in extreme cases backwards motion when facing an oncoming pedestrian head-on. Such behavioral responses to encountering pedestrians head-on typically apply to humans as well, since it is uncommon for pedestrians to walk backwards. The policy of side-stepping is accomplished by prohibiting velocity in the opposite direction of the attractive goal point and by creating an enforcing effect on the velocity in the perpendicular direction. The perpendicular movement increase is governed by a ratio $\lambda = \frac{\mathbf{F}_{\alpha\beta}(x)}{\mathbf{F}_{\alpha\beta}(y)}$ where x is direction away from goal and y is direction perpendicular to x. If the resultant velocity from the external forces point away from the goal point and the ratio is larger than a threshold, then $\mathbf{F}_{\alpha\beta}(y) = \mathbf{F}_{\alpha\beta}(y) * \lambda$.

*3) **Following Behavior**:* The third augmentation developed for the ASFM allows to start following a pedestrian showing the same directional intention, after the model has encountered any repulsive forces as a means to overcome freezing or stopping up after having encountered a seemingly blocked path and then never progress beyond that point. Following someone else is a very common pedestrian behavior when encountering densely populated areas or narrow pathways. Recognizing a pedestrian as having the same immediate goal as the robot can be done by analyzing their direction of motion. Once a pedestrians direction of motion is determined, the angle between the robot system and the pedestrian direction can be calculated, and if it is within a certain range the robot can assume the pedestrian is walking in the same direction as the robot wants to go. Once a pedestrian is determined to be fit to follow, the goal is set to the pedestrians location as to make the robot follow.

When a pedestrian follows other pedestrians through a crowded area, they stop following anyone as soon as there is no need for it anymore and resume the pursuit of their own goal. Therefore the robot must also be able to judge when to stop following the pedestrian they have started following. The policy implemented for the follow mode set a timer when the robot is following someone and they no longer experience any external repulsive forces – the area is no longer crowded. Once the timer is up the robot will again walk towards its original goal. the robot also stops following a pedestrian if the pedestrian being followed is more than threshold distance away. A diagram of the full follow pedestrian procedure can be seen in Fig. 2b.

*4) **Direction Priority**:* The fourth augmentation developed for the ASFM is to negate any force influence from pedestrians moving away from the robot. One of SFM's shortcomings was its approach of lowering repulsive forces using the direction dependent weighting function. For a first person POV, this function is not very reliable as vision is limited. Annulling any repulsive force coming from pedestrians that are moving away from the robot requires the robot to log the position of detected humans and compare their latest logged position to their current position in order to gauge if the pedestrian is moving away from the robot. This approach is very useful for a first person field of view robot as it does not need to take into consideration the movement of the robot. If

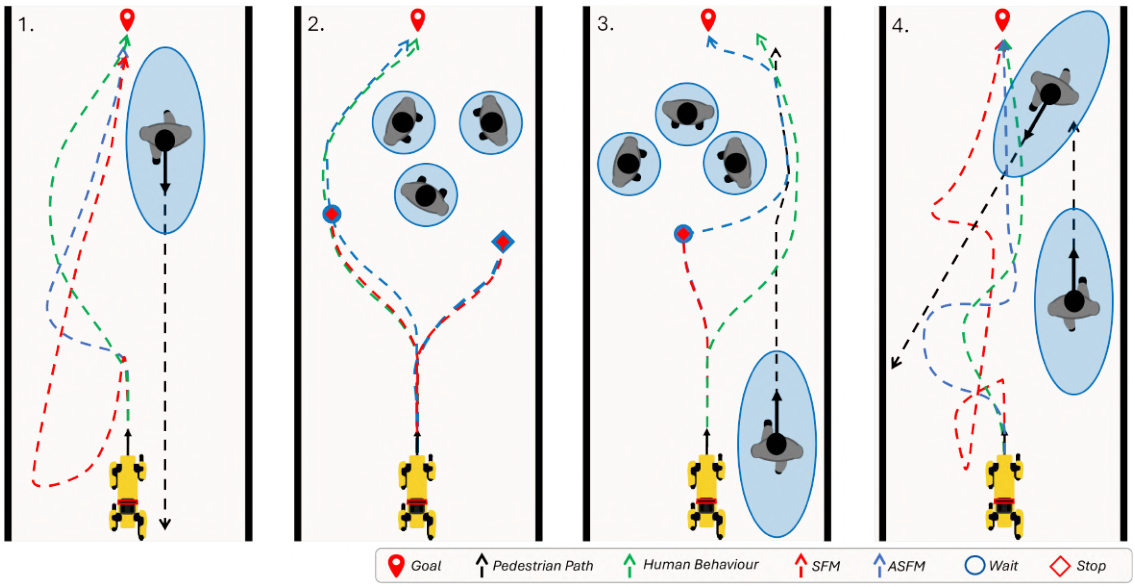

Fig. 4: Setup visualization along with the resultant behavior of a human pedestrian (green), the robot using ASFM (blue), and the standard SFM (red) in all four navigation scenarios.

the robot is moving and a person is going further away from the robot from one instance to another, then it means the pedestrian is walking faster than the robot and it is a valid assumption to ignore the repulsive forces from the pedestrian.

5) ***Human Adaptive Velocity Control****:* The fifth augmentation created for the ASFM regulates the robots velocity based on the distance of any human. With the robot system and camera, the SFM model would often experience the max robot velocity to be too fast for the latency in deceleration when interacting with other pedestrians. Therefore the last proposed augmentation to the ASFM is a reduction in max velocity based on how far away from the robot the closest detected pedestrian is. This max velocity system creates a more pedestrian friendly behavior when approaching a pedestrian head on. An illustration of the max velocity zone system can be seen in Fig. 2c with values that were deemed most appropriate through experiments.

IV. EXPERIMENTAL SETUP

A. Robot System Description

The developed system could be applied to any omnidirectional mobile robot. In this paper, a quadruped robot (Spot) was used, equipped with a ZED2i stereo camera. Even though robots, such as Spot, have local collision avoidance onboard, these assume static environments without social navigation awareness of moving humans; such functionalities were deactivated when running the ASFM. The robot's onboard computer was not used for any high-level navigation, although an Nvidia Jetson Orin 32GB edge GPU was used onboard to run the ASFM, mainly needed for the human-localization. For inferring the position and velocities of humans around the robot, the StereoLabs tailored human pose detection model for the ZED2i stereo camera. The system runs in real-time at 15 frames per second for human pose detection. On the robot, the ZED2i camera is placed on a custom stand on the robot's back that elevates the stereo camera to $1.1m$ above the ground to get a better view of pedestrians close to the robot. The SFM itself does not require GPU to run in real-time. The system integration can be seen in Fig. 3.

The path planning approach of the navigation model was based on predetermined checkpoints that have been recorded in the robot's odometry frame in advance, for the given environment that the robot is set to navigate through. This type of navigation was chosen to replicate an inspection task or a preset delivery route. Thus the robot goes from checkpoint to checkpoint with the condition of coming within one meter distance away from the coordinates of the current checkpoint goal before it sets the goal to the next checkpoint.

B. Navigation Scenarios Setup

We tested ASFM vs SFM over four scenarios. To invoke all the different pedestrian interaction scenarios ASFM can react to, the setup involved a narrow 2.1m wide hallway, where the robot had to maneuver around various crowd formations and common interactions towards a goal point located 8.5m from its starting position. A hallway restricts movement except in the direction towards the next goal point and so was chosen as the most convenient test location. The four experiments were attempted 20 times for each algorithm.

The first navigation scenario was aimed at testing the ability of the ASFM compared to SFM to involve an oncoming pedestrian, while maintaining a set trajectory towards the goal point. This scenario was designed to test the model's effectiveness in mimicking human-like behavior in terms of sidestepping to avoid a collision without significant reduction in speed.

In the second navigation scenario, the objective was to evaluate the ASFM vs the standard SFM in their ability to

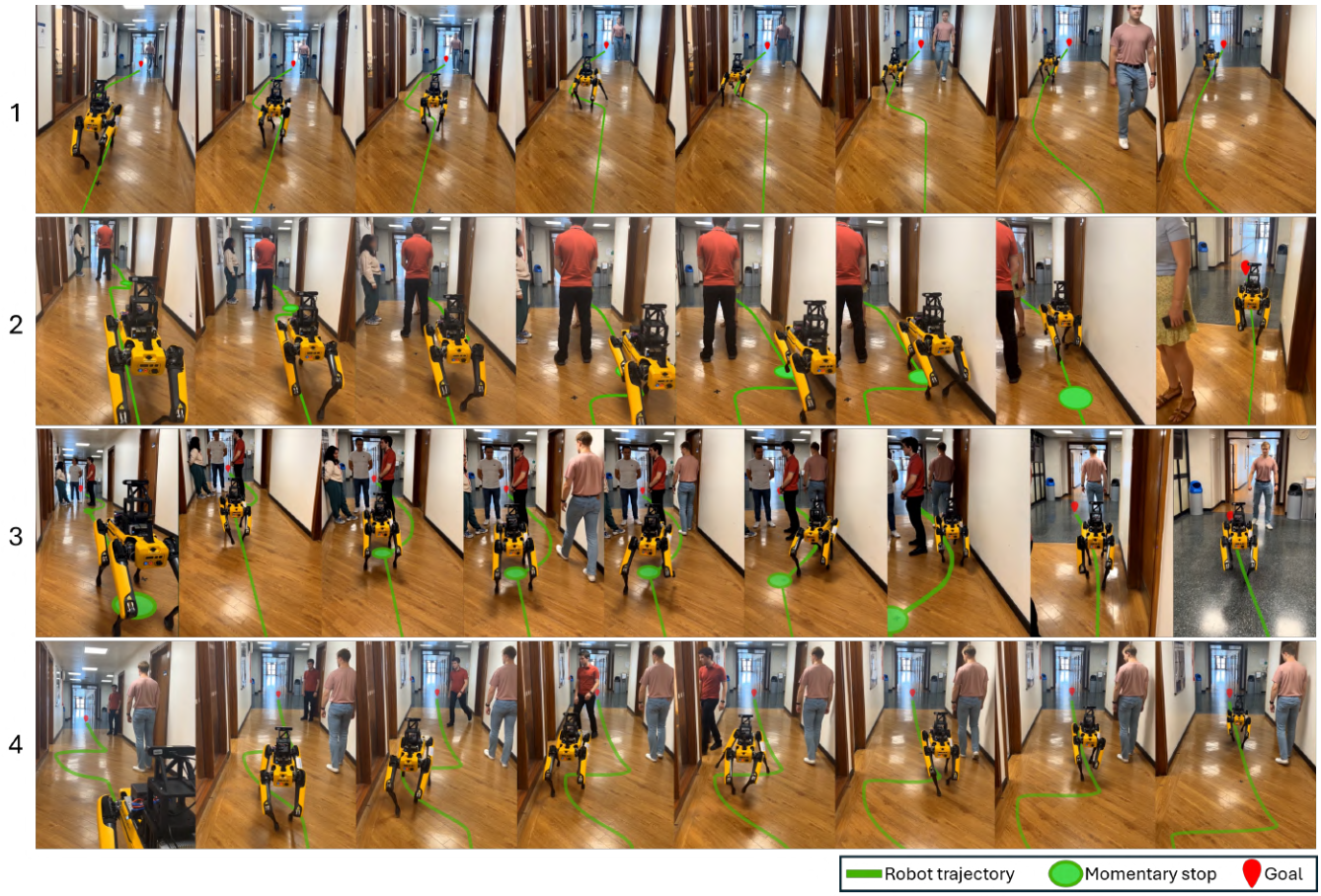

Fig. 5: Visual illustration of a robot pedestrians using ASFM for all four experimental scenarios. The green line illustrates the path the robot takes, the red pointer is the goal pose, and the green circle signifies position of momentary stop.

navigate through static crowd formations within a confined space. This scenario involved a robot encountering a static crowd of three individuals blocking a significant portion of the hallway, which closely mimics real-life situations where pedestrians must maneuver around stationary groups. The real-life equivalent would typically involve a pedestrian choosing a path that offers the least resistance and space consumption. The experiment aimed to assess the models' performance in identifying and utilizing the most viable pathway around the static crowd to reach a designated endpoint.

In the third navigation scenario, the complexity increased as we aimed to evaluate the model's performance in situations where the robot had to navigate through an environment with an obstructed pathway, requiring the robot to follow a pedestrian to find a clear path. This scenario was intended to mimic real-world situations where a pedestrian navigates through crowded areas by following others.

In fourth navigation scenario, the focus was on evaluating the ASFM and standard SFM in complex dynamic environments involving two pedestrians with differing speeds and intentions. Specifically, the robot faced challenges including an unseen pedestrian crossing its path unexpectedly and another pedestrian moving slower than the robot itself. This setup aimed to simulate real-world cases where a robot must dynamically adjust to sudden changes in its environment and overtake slower-moving pedestrians without compromising social comfort or safety.

V. RESULTS

An overview of the outcomes from the four navigation scenarios utilizing the ASFM, as depicted in Figs. 4 and 5. Additionally, we present a comparative analysis of the ASFM's performance against that of the traditional SFM, illustrated in Fig. 6. To determine the statistical significance of the ASFM's enhanced performance, paired T-tests were executed, with the results detailed in Table I. The assessment of pedestrian comfort, a critical factor in social robotics, was predicated on the criterion that individuals were not required to deviate substantially from their intended paths due to the robot's presence. This qualitative measure was gauged through systematic observations. Further, comprehensive video demonstrations showing the ASFM's navigational strategies and interactions can be accessed via the following link: `https://rpl-cs-ucl.github.io/ASFM`.

Scenario 1: Both the ASFM and SFM secured a 100% goal arrival rate, aligning with the experiment's simplicity. However, ASFM outperformed SFM in efficiency, evidenced

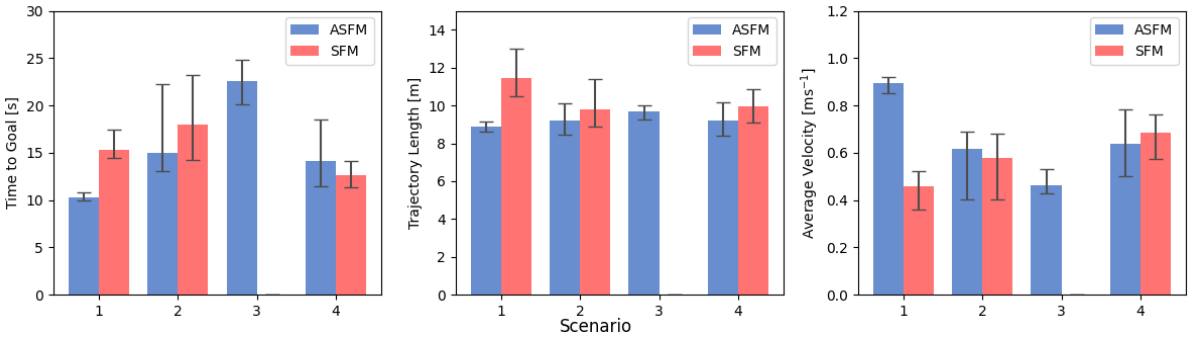

Fig. 6: Performance comparison between ASFM and SFM in time to goal, average velocity, and the trajectory length. ASFM performs faster at a higher velocity for simple scenarios, and is slower in more complex scenarios which indicates a lower level of intrusion on surrounding pedestrians. SFM is not presented in Scenario 3, as it had 0% success rate.

by quicker goal attainment, enhanced path efficiency, and reduced path irregularity, as depicted in Fig. 6. Table I shows significant improvements in ASFM's time to goal, trajectory length, and average velocity for scenario 1, with T-statistics of $33.464, -57.109$, and 20.360, respectively. Notably, ASFM demonstrated improved social navigation by facilitating more natural sidestepping and maintaining pedestrian comfort without necessitating path alterations, thus mirroring more human-like behaviors. These findings underscore the enhanced performance of the ASFM in facilitating more efficient and socially acceptable robot navigation in environments with pedestrian traffic.

Scenario 2: While both models avoided collisions, the ASFM demonstrated a superior arrival rate of 75% compared to the SFM's 40%, highlighting the ASFM's enhanced ability to interpret and navigate through crowded spaces. ASFM exhibited significant improvements in time to goal and average velocity with T-statistics of $T = 5.855$ and $T = 4.085$. Despite this, both models occasionally struggled with accurately interpreting the crowd's formation, leading to varied success rates and indicating a potential area for improvement in crowd understanding. The findings from this scenario underline the challenges and complexities associated with automated navigation through densely populated environments, showcasing the ASFM's relative advantage in handling static human obstacles compared to the conventional SFM.

Scenario 3: The standard SFM failed to navigate through the crowd with an arrival rate of 0%. The ASFM, however, achieving an 85% success rate in following a pedestrian and effectively bypassing the crowd. The failure of SFM was mainly due to the complexity of having static and moving human crowds, the SFM cannot deal without side stepping. The success of the ASFM can be attributed to its enhanced ability to interpret pedestrian intentions and movements, allowing it to utilize social cues to navigate through tight spaces. However, there were instances of failure due to limitations in pedestrian detection, indicating areas for future improvement in sensor capabilities and model responsiveness. Overall, this scenario underscored the ASFM's superior performance in complex social navigation tasks, showcasing its potential for real-world applications in crowded environments.

Scenario 4: Both models maintained a 100% arrival rate. However, the SFM struggled with evasive maneuvers and maintaining an appropriate distance from the slow-moving pedestrian, often resulting in socially awkward or uncomfortable encounters. This was primarily due to the SFM's limitations in responding non-intrusively to the oncoming pedestrian, compelling them to alter their trajectories. In contrast, the ASFM exhibited superior adaptability, maintaining a safer distance and implementing more natural sidestepping behaviors in response to crossing pedestrians. Statistical analysis revealed that the ASFM achieved significant improvements in time to goal ($T = -2.508$) and average velocity ($T = 5.580$), although no significant difference was found in trajectory length ($T = 1.808$) between the two models. This suggests the ASFM enhances social navigation but needs further optimization for better efficiency and adaptability in dynamic settings.

TABLE I: T-test results for, time, velocity, and travel distance.

Parameter	Navigation Scenario	T-statistic	P-value
Time to Goal	1	33.464	< 0.05
	2	5.855	< 0.05
	3	n/a	n/a
	4	-2.508	< 0.05
Trajectory Length	1	-57.109	< 0.05
	2	-3.535	< 0.05
	3	n/a	n/a
	4	1.808	ns
Average Velocity	1	20.360	< 0.05
	2	4.085	< 0.05
	3	n/a	n/a
	4	5.580	< 0.05

ns = no significance.
n/a = not applicable

These findings underscore the ASFM's capacity to significantly improve robotic navigation in pedestrian settings, demonstrating its utility in enhancing key navigation metrics across varied scenarios. The mixed outcomes in navigation scenario 4 highlight the model's context-sensitive performance, suggesting further model optimization is necessary for consistent across-the-board improvements.

VI. CONCLUSION AND FUTURE WORK

A model for social navigation using vision was developed for mobile robots, implemented on a quadruped and enabling safe and comfortable movement through pedestrian environments. Improvements over the standard SFM were made by incorporating the ASFM, addressing limitations in pedestrian formation awareness and sensory input. Enhancements such as direction prioritization, pedestrian path avoidance, and the ability to follow a guide through dense crowds were included. Real-world applicability was increased, pedestrian reactions were reduced, and human-robot interaction was improved. In future work the generalization to more diverse and larger-scale environments is aimed, as well as enhancing the model's scalability to more complex environments or higher pedestrian densities.

REFERENCES

[1] S. LaValle, *Planning Algorithms*. Cambridge University Press, 2006.

[2] X. Feng *et al.*, "Computer Vision Algorithms and Hardware Implementations: A Survey," *Integration*, vol. 69, pp. 309–320, 2019.

[3] S. Rosa *et al.*, "Tour Guide Robot: a 5G-Enabled Robot Museum Guide," *Frontiers in Robotics and AI*, vol. 10, 2024.

[4] H. Chai *et al.*, "A survey of the development of quadruped robots: Joint configuration, dynamic locomotion control method and mobile manipulation approach," *BIROB*, vol. 2, no. 1, p. 100029, 2022.

[5] T. Peng *et al.*, "Learning Bipedal Walking on a Quadruped Robot via Adversarial Motion Priors," in *TAROS*, 2023.

[6] C. I. Mavrogiannis *et al.*, "Core Challenges of Social Robot Navigation: A Survey," *CoRR*, vol. abs/2103.05668, 2021.

[7] S. Thrun *et al.*, "MINERVA: a Second-Generation Museum Tour-Guide Robot," in *IEEE ICRA*, vol. 3, 1999, pp. 1999–2005.

[8] M. Stamatopoulou *et al.*, "DiPPeST: Diffusion-based Path Planner for Synergistic Trajectory Generation Applied on Quadrupedal Robots," in *IEEE/RSJ IROS*, 2024.

[9] J. Liu *et al.*, "DiPPeR: Diffusion-based 2D Path Planner applied on Legged Robots," in *IEEE ICRA*, 2024.

[10] V. Suryamurthy *et al.*, "Terrain Segmentation and Roughness Estimation using RGB Data: Path Planning Application on the CENTAURO Robot," in *IEEE/RAS Humanoids*, 2019.

[11] L. Yao *et al.*, "Local navigation among movable obstacles with deep reinforcement learning," in *IEEE/RSJ IROS*, 2023.

[12] K. Ellis *et al.*, "Navigation Among Movable Obstacles with Object Localization using Photorealistic Simulation," in *IEEE IROS*, 2023.

[13] ——, "Navigation Among Movable Obstacles via Multi-Object Pushing into Storage Zones," *IEEE Access*, 2023.

[14] D. Kanoulas *et al.*, "Curved patch mapping and tracking for irregular terrain modeling: Application to bipedal robot foot placement," *Robotics and Autonomous Systems*, 2017.

[15] V. S. Raghavan *et al.*, "Variable Configuration Planner for Legged-Rolling Obstacle Negotiation Locomotion: Application on the CENTAURO Robot," in *IEEE/RSJ IROS*, 2020.

[16] J. Liu *et al.*, "ViT-A*: Legged Robot Path Planning using Vision Transformer A*," in *IEEE-RAS Humanoids*, 2023.

[17] B. D. Ziebart *et al.*, "Planning-based Prediction for Pedestrians," in *IEEE/RSJ IROS*, 2009, pp. 3931–3936.

[18] K. Li *et al.*, "Socially aware crowd navigation with multimodal pedestrian trajectory prediction for autonomous vehicles," in *IEEE ITSC*, 2020, pp. 1–8.

[19] H. Kretzschmar, M. Spies, C. Sprunk, and W. Burgard, "Socially compliant mobile robot navigation via inverse reinforcement learning," *IJRR*, vol. 35, no. 11, pp. 1289–1307, 2016.

[20] G. F. Cooper, "The computational complexity of probabilistic inference using bayesian belief networks," *Artificial Intelligence*, vol. 42, no. 2, pp. 393–405, 1990.

[21] C. I. Mavrogiannis, V. Blukis, and R. A. Knepper, "Socially competent navigation planning by deep learning of multi-agent path topologies," in *IEEE/RSJ IROS*, 2017, pp. 6817–6824.

[22] E. Stein, J. S. Birman, J. N. Mather *et al.*, *Braids, Links, and Mapping Class Groups*. Princeton University Press, 1974, no. 82.

[23] S. Russell, "Learning agents for uncertain environments," in *COLT*, 1998, pp. 101–103.

[24] A. Mohamed, K. Qian, M. Elhoseiny, and C. Claudel, "Social-stgcnn: A social spatio-temporal graph convolutional neural network for human trajectory prediction," in *IEEE/CVF CVPR*, 2020.

[25] Y. F. Chen *et al.*, "Socially Aware Motion Planning with Deep Reinforcement Learning," in *IEEE/RSJ IROS*, 2018.

[26] N. Hirose *et al.*, "Sacson: Scalable autonomous control for social navigation," *IEEE RA-L*, vol. 9, no. 1, pp. 49–56, 2024.

[27] A. Gupta, J. Johnson, L. Fei-Fei, S. Savarese, and A. Alahi, "Social gan: Socially acceptable trajectories with generative adversarial networks," in *IEEE CVPR*, 2018, pp. 2255–2264.

[28] T. Bandyopadhyay *et al.*, "Intention-aware motion planning," in *Algorithmic foundations of robotics X*. Springer, 2013, pp. 475–491.

[29] C. Choi *et al.*, "Drogon: A trajectory prediction model based on intention-conditioned behavior reasoning," *arXiv:1908.00024*, 2019.

[30] D. Helbing and P. Molnár, "Social Force Model for Pedestrian Dynamics," *Physical Review E*, vol. 51, no. 5, pp. 4282–4286, 1995.

[31] A. Alahi *et al.*, "Social lstm: Human trajectory prediction in crowded spaces," in *IEEE CVPR*, 2016, pp. 961–971.

[32] T. Yagi *et al.*, "Future person localization in first-person videos," in *IEEE CVPR*, 2018.

[33] F. Farina *et al.*, "Walking Ahead: The Headed Social Force Model," *PLOS ONE*, vol. 12, no. 1, pp. 1–23, 01 2017.

[34] M. Boldrer *et al.*, "Socially-Aware Reactive Obstacle Avoidance Strategy Based on Limit Cycle," *IEEE RA-L*, vol. 5, no. 2, 2020.

[35] ——, "Multi-agent Navigation in Human-shared Environments: A Safe and Socially-aware Approach," *RAS*, vol. 149, 2022.